RAPPORT

IRSN
INSTITUT
DE RADIOPROTECTION
ET DE SÛRETÉ NUCLÉAIRE

Rapport final du projet RAP 2008

Effets de l'atténuation anélastique sur la réponse des sols et estimation probabiliste site-spécifique du mouvement sismique

DEI/SARG/2010-035

DIRECTION DE L'ENVIRONNEMENT
ET DE L'INTERVENTION

Service d'analyse des risques liés à la géosphère

Géosciences pour une Terre durable
brgm

ERA-R
Equipe de Recherche associée au LCPC
Risque Sismique

Système de management
de la qualité IRSN certifié

IRSN
INSTITUT
DE RADIOPROTECTION
ET DE SÛRETÉ NUCLÉAIRE

DIRECTION DE L'ENVIRONNEMENT ET DE L'INTERVENTION

Service d'analyse des risques liés à la géosphère

BP 17 - 92262 Fontenay-aux-Roses Cedex France

Demandeur	Réseau Accélérométrique Permanent (GIS-RAP)
Référence de la demande	Convention inter-établissement Programme de Recherche GIS-RAP
Numéro de la fiche programme	01D/T04-004/01
Processus de rattachement	R4

Effets de l'atténuation anélastique sur la réponse des sols et estimation probabiliste site-spécifique du mouvement sismique

L.F. Bonilla[(1)], C. Gélis[(1)], J. Douglas[(2)], P. Gehl[(2)], J. Régnier[(3)], E. Bertrand[(3)], A.-M. Duval[(3)]

(1) Institut de Radioprotection et de Sûreté Nucléaire

(2) Bureau des Recherches Géologiques et Minières

(3) CETE-Méditerranée

Rapport DEI/SARG/2010-035

	Réservé à l'unité		Visas pour diffusion		
	Auteur(s)	Vérificateur(s)	Chef du **SARG**	Directeur de la **DEI**	Directeur Général de l'**IRSN**
Noms	L.F. Bonilla	D. Baumont	D. GAY	D. CHAMPION	J. REPUSSARD
Dates	30/07/2010	30/07/2010	27/09/2010	30/09/2010	
Signatures	F. Bonilla	D. B			

DIFFUSION : Libre ☒ Interne ☐ Limitée ☐

IRSN
INSTITUT
DE RADIOPROTECTION
ET DE SÛRETÉ NUCLÉAIRE

RESUME

DANS LE CADRE DE L'APPEL D'OFFRE RAP-2008, L'IRSN, LE BRGM, LE LGIT ET LE CETE-MEDITERRANEE SE SONT ASSOCIES POUR TRAVAILLER SUR DES SUJETS CONCERNANT LES EFFETS DE SITE. CE PROJET COMPORTE DEUX VOLETS : (1) ESTIMATION DES EFFETS DE L'ATTENUATION ANELASTIQUE (KAPPA) POUR AMELIORER L'EVALUATION DE L'EFFET DE SITE : APPLICATION SUR DES STATIONS ACCELEROMETRIQUES RAP, (2) ESTIMATION CONJOINTE DE L'ALEA SISMIQUE PROBABILISTE POUR UN SITE SPECIFIQUE ET DES EFFETS DE SITE 1D ET 2D.

MOTS-CLES

EFFETS DE SITE, RAP

SOMMAIRE

1 INTRODUCTION

Durant l'année 2008, le Groupement d'Intérêt Scientifique du Réseau Accélérométrique Permanent (GIS-RAP) a fait appel aux chercheurs en France pour recueillir des propositions d'études et de recherche sur le risque sismique. Ainsi, l'IRSN, le BRGM, le LGIT et le CETE Méditerranée se sont associés pour travailler ensemble pendant un an sur des sujets concernant les effets de site. Le projet proposé vise à améliorer la modélisation des effets de site dans l'estimation du mouvement sismique et de l'aléa sismique. Ce projet comporte deux volets : (1) Estimation des effets de l'atténuation anélastique (kappa) pour améliorer l'évaluation de l'effet de site : application sur des stations accélérométriques RAP, (2) Développement d'une méthode pour l'évaluation probabiliste de l'aléa sismique en incluant les effets de site 1D et 2D. Les personnes impliquées dans le projet sont :

- IRSN : Fabian Bonilla et Céline Gélis
- BRGM : John Douglas et Pierre Gehl
- LGIT : Céline Beauval et Héloïse Cadet
- CETE : Julie Régnier, Etienne Bertrand et Anne-Marie Duval

Fabian Bonilla de l'IRSN a été désigné coordinateur du projet. Le budget alloué par le bureau du RAP à ce projet est de 7000 €, montant qui a essentiellement servi la prise en charge des frais associés aux réunions techniques entre partenaires.

Le présent document constitue le rapport final du projet et décrit brièvement les travaux réalisés. Ce travail a été valorisé à travers une publication scientifique parue dans PAGEOPH et une communication orale dans un congrès international avec la publication d'un résumé étendu. Ces documents sont attachés en annexe.

2 ESTIMATION DES EFFETS DE L'ATTENUATION ANELASTIQUE (KAPPA) POUR AMELIORER L'AVALUATION DE L'EFFET DE SITE : APPLICATION SUR DES STATIONS ACCELEROMETRIQUES RAP

Le mouvement sismique enregistré à certaines stations peut être significativement modifié par les conditions locales du site. Un des paramètres contrôlant le niveau d'amplification est l'atténuation anélastique du milieu. Dans le calcul empirique du mouvement sismique, cette atténuation est généralement décomposée en un facteur d'atténuation régional (Qs) et un facteur lié aux conditions locales du site (kappa) (Anderson and Hough, 1984). Un précédent projet RAP (Douglas et al., 2008) a permis d'estimer l'effet de site en utilisant différents degrés de connaissance du milieu. L'amplification y a été calculée à travers la méthode « quater wavelength » (Joyner et al., 1981), donnant une amplification du mouvement sismique pour chaque fréquence. Dans cette méthode, l'atténuation est prise en compte à travers le facteur kappa. Les résultats de cette étude montrent que la valeur de kappa influence fortement l'amplitude spectrale à hautes fréquences et par conséquent l'amplification du mouvement sismique.

Kappa est aussi un paramètre très important dans les méthodes stochastiques de simulation du mouvement sismique. Ces méthodes sont très utilisées dans des régions où les données de mouvement fort sont insuffisantes. Différentes études réalisées aux Etats-Unis montrent que kappa varie à l'echelle régionale en fonction des conditions géologiques. Ainsi, la Californie (région tectoniquement active avec un substratum ayant des proprietés mécaniques relativement faibles) se caractérise par une valeur de kappa proche de 0,04 s. La côte est (région tectonique stable avec un substratum ayant des proprietés mécaniques dures) a une valeur de kappa d'environ 0,006 s. Ainsi, pour un couple magnitude/distance donné, le mouvement sismique est plus important dans les régions continentales stables (les hautes frequences étant moins atténuées) que dans les régions actives.

L'objectif de cette étude consiste à évaluer le facteur kappa en analysant les données enregistrées par le Réseau Accélérométrique Permanent (RAP) en France. Compte tenu du nombre de données disponibles, trois régions ont été sélectionnées : les Pyrénées, les Alpes et la Côte d'Azur. Les résultats montrent que la valeur moyenne de kappa est comprise, en général, entre les valeurs calculées pour la Californie et la côte ouest des Etats-Unis. Plus particulièrement, la valeur de kappa estimée sur les sites au rocher dans la région des Alpes est de 0,0254 s ; valeur proche de celle obtenue par d'autres études dans cette zone.

Les résultats de ce travail ont été publiés dans le journal Pure and Applied Geophysics (PAGEOPH). L'article correspondant est joint en Annexe 1.

3 DEVELOPPEMENT D'UNE METHODE POUR L'EVALUATION PROBABILISTE DE L'ALEA SISMIQUE EN INCLUANT LES EFFETS DE SITE 1D ET 2D

L'estimation probabiliste de l'aléa sismique (Probabilistic Seismic Hazard Assessment, PSHA) est aujourd'hui une méthodologie de référence pour le dimensionnement des structures. En effet, l'Eurocode 8, le nouveau code de construction parasismique en Europe, est désormais basé sur des études probabilistes. Si le PSHA est la méthodologie de base pour les nouveaux zonages sismiques pour chaque pays d'Europe, les études d'aléa sismique spécifiques à un site demeurent cependant essentiellement déterministes. Néanmoins, une étude probabiliste peut être requise dans le cas des bâtiments à intérêt particulier ou « à risque spécial », tels que les hôpitaux, les barrages, les installations nucléaires de base, etc. Lors qu'un site particulier est examiné, une étude « site-spécifique » doit être menée. Ce type d'étude permet d'évaluer un spectre de réponse uniforme (Uniform Hazard Spectrum, UHS), c'est à dire un spectre pour lequel chaque amplitude a la même probabilité d'être dépassée sur une période de temps donnée. Ces études reposent, en général, sur des équations empiriques pour la prédiction du mouvement sismique. De ce fait, la prise en compte des effets de site dans l'évaluation des spectres de réponse découle directement des hypothèses retenues pour établir les équations empiriques utilisées (via les coefficients de site, fréquence de résonance).

L'objectif de cette étude est de poursuivre le développement d'une méthode de calcul de l'aléa probabiliste en incluant les effets de site. Ceci est une prolongation de l'étude RAP 2008 (Régnier et

al., 2008) qui avait permis d'analyser la variabilité de la réponse 1D de sites RAP à Nice. Dans ce projet, nous nous concentrons sur la variabilité spatiale du mouvement sismique. Pour ce faire, nous étudions la propagation des ondes sismiques dans un milieu hétérogène linéaire et non linéaire à deux dimensions.
Le présent travail inclut une analyse de la réponse sismique d'une section 2D du bassin de Nice. Les principaux résultats montrent d'une part que le contraste d'impédance domine l'amplification, et d'autre part que l'effet de la géométrie 2D du bassin peut être entre 4 et 5 fois plus fort que sa réponse 1D. Enfin, ce travail a révélé que l'amplification dépend fortement de l'angle d'incidence du champ sismique indépendamment de la rhéologie du matériel de remplissage.

Les résultats de ce travail ont été présentés lors de la Conférence *Seismic Risk 2008 - Earthquakes in North-Western Europe*, 11-12 September 2008, Liège, Belgium et publiés dans les proceedings sous la forme d'un résumé étendu (Annexe 2).

4 ANNEXE 1 : A KAPPA MODEL FOR MAINLAND FRANCE

Pure Appl. Geophys.
© 2010 Birkhäuser / Springer Basel AG
DOI 10.1007/s00024-010-0146-5

Pure and Applied Geophysics

A κ Model for Mainland France

John Douglas,[1] Pierre Gehl,[1] Luis Fabian Bonilla,[2] and Céline Gélis[2]

Abstract—An important parameter for the characterization of strong ground motion at high-frequencies (>1 Hz) is kappa, κ, which models a linear decay of the acceleration spectrum, $a(f)$, in log-linear space (i.e. $a(f) = A_0 \exp(-\pi \kappa f)$ for $f > f_E$ where f is frequency, f_E is a low frequency limit and A_0 controls the amplitude of the spectrum). κ is a key input parameter in the stochastic method for the simulation of strong ground motion, which is particularly useful for areas with insufficient strong-motion data to enable the derivation of robust empirical ground motion prediction equations, such as mainland France. Numerous studies using strong-motion data from western North America (WNA) (an active tectonic region where surface rock is predominantly soft) and eastern North America (ENA) (a stable continental region where surface rock is predominantly very hard) have demonstrated that κ varies with region and surface geology, with WNA rock sites having a κ of about 0.04 s and ENA rock sites having a κ of about 0.006 s. Lower κs are one reason why high-frequency strong ground motions in stable regions are generally higher than in active regions for the same magnitude and distance. Few, if any, estimates of κs for French sites have been published. Therefore, the purpose of this study is to estimate κ using data recorded by the French national strong-motion network (RAP) for various sites in different regions of mainland France. For each record, a value of κ is estimated by following the procedure developed by Anderson and Hough (Bull Seismol Soc Am 74:1969–1993, 1984): this method is based on the analysis of the S-wave spectrum, which has to be performed manually, thus leading to some uncertainties. For the three French regions where most records are available (the Pyrenees, the Alps and the Côtes-d'Azur), a regional κ model is developed using weighted regression on the local geology (soil or rock) and source-to-site distance. It is found that the studied regions have a mean κ between the values found for WNA and ENA. For example, for the Alps region a κ value of 0.0254 s is found for rock sites, an estimate reasonably consistent with previous studies.

Key words: Strong-motion data, kappa, high-frequency decay, France, RAP, near-surface attenuation.

1. Introduction

As is the case for many regions with limited observational ground motion databases, seismic hazard assessment in France is complicated by large epistemic uncertainty concerning the expected ground motion in future earthquakes. Thanks to the establishment in the past couple of decades of a reasonably dense national strong-motion network in the most seismically active parts of France (the Réseau Accélérometrique Permanent, RAP) many thousands of accelerometric records are now freely available (Péquegnat *et al.*, 2008). Nevertheless, due to the relatively low earthquake occurrence rates in mainland France there are very few records from earthquakes with moment magnitude, M_w, greater than 5.0. Due to recognized differences in magnitude- and distance-scaling of ground motions from small and large earthquakes (e.g. Bommer *et al.*, 2007; Cotton *et al.*, 2008, and references therein) it is currently not possible to develop robust, fully-empirical ground motion prediction equations (GMPEs) reliable for higher magnitudes based on these data. Three alternative methods for the estimation of earthquake ground motions in France could be applied: (1) assume that ground motions in France are similar to those in areas for which robust GMPEs (either empirical or simulation-based) have been proposed (e.g. California, Japan or Italy) (e.g. Cotton *et al.*, 2006); (2) develop simulation-based GMPEs using input parameters derived from seismological analyses, as, for example, have been developed for eastern North America (e.g. Atkinson and Boore,

John Douglas is currently on teaching leave at Earthquake Engineering Research Centre, University of Iceland, Austurvegur 2A, 800 Selfoss, Iceland.

[1] BRGM, RNSC/RIS, 3 avenue C. Guillemin, BP 36009, 45060 Orléans Cedex 2, France. E-mail: j.douglas@brgm.fr

[2] IRSN, DEI/SARG/BERSSIN, BP 17, 92262 Fontenay-aux-Roses, France.

Published online: 20 April 2010

2006); or (3) adjust GMPEs developed for other regions to be more applicable to France through, for example, the hybrid empirical-stochastic technique (e.g. Campbell, 2003; Douglas *et al*., 2006) or the referenced empirical approach (Atkinson, 2008). Up until now method 1 has been used almost universally for France, probably due to the lack of sufficient strong-motion data from which to derive input parameters required for methods 2 and 3. Methods 2 and 3 generally require estimating various parameters characterizing the earthquake source (e.g. the stress drop parameter $\Delta\sigma$ and the source spectral shape), the travel path (e.g. geometrical decay and Q) and the local site (e.g. shear-wave velocity profile and near-surface attenuation). Numerous previous studies have estimated one or more of these parameters for France or regions of France (e.g. Campillo *et al*., 1993; Drouet *et al*., 2005, 2008). However, we know of no published studies explicitly reporting estimates of κ as introduced by Anderson and Hough (1984). The site contribution to κ is commonly believed to be related to the attenuation (e.g. Q or damping) in the top couple of kilometers, although there is some evidence for decay of high frequencies due to source properties related to the size of a cohesive zone at the crack tip (e.g. Papageorgiou and Aki, 1983; Tsai and Chen, 2000). The effect of κ is to act as a high-frequency (>1 Hz) filter on ground motions and, therefore, it is a critical parameter for the accurate estimation of, for example, peak ground acceleration. Consequently, in this article we estimate κ using hundreds of accelerometric records from mainland France.

One motivation for this study was the finding of Douglas *et al*. (2009), who presented an approach to constrain the shear-wave velocity profile by making use of all available information on site conditions at a site of interest (e.g. soil type and depth to bedrock). They found that even when the shear-wave velocity profile is precisely known, the high-frequency site amplification is not. Douglas *et al*. (2009) attributed this, at first sight surprising, result to a lack of constraint on the near-surface attenuation. In their analysis they modelled attenuation by κ estimated using the empirical relationship of Silva *et al*. (1998) connecting κ and $V_{s,30}$ (the average shear-wave velocity of the top 30 m); this relationship had a large associated standard deviation that led to the large uncertainty in the high-frequency site amplification. If κ could be better estimated at a given site then there is the potential to significantly reduce this uncertainty. Therefore, in this article we investigate κ to see whether it can be better constrained for French sites.

This article starts with a section describing the strong-motion data used; next we describe our method for the evaluation of κ from the Fourier spectra of these data including an approach to estimate the accuracy of the estimated κs due to the subjectivity of the adopted methodology; following that we investigate the dependence of κ on source-to-site distance, region and local site conditions; and finally we conclude.

2. Data Used

In order to concentrate on data of engineering interest and to limit the number of records analyzed, only records from earthquakes with magnitudes (any scale) larger than about 3.5 were downloaded from the RAP online strong-motion database (http://www-rap.obs.ujf-grenoble.fr/). Each acceleration time-history was then visually inspected and poor quality records (due to noise or severe baseline problems) on any of the three components were rejected from further consideration. In total, 263 triaxial records (i.e. 789 components) from 30 earthquakes and 83 different stations were retained for analysis (Table 1; Fig. 1). Note that κs were computed for all three components. Earthquake locations given in the RAP database were used here since these are from local networks (mainly the French national RéNaSS catalogue) and, in addition, most available data are from considerable source-to-site distances and, therefore, accurate hypocentral locations are not critical for this analysis.

Most of the records selected were recorded by stations in the three most seismically active regions of France: the Pyrenees (109 records), the Alps (88 records) and the Côtes-d'Azur (50 records) (although sometimes the earthquake recorded occurred in a different region). Possible regional dependence of κ between these different areas is examined in Sect. 5.

Table 1

Earthquakes and stations used to compute κ

YYYY	MM	DD	HH	MIN	Lat.(N)	Lon.(E)	M_w	Stations	NS
1996	02	18	04	16	44.74	6.77	3.4 (m_b, ISC)	OGAG	1
1996	07	15	00	13	46.00	6.11	5.3 (CSEM)	OGAG, OGDH, OGSI, SAOF	4
1996	07	23	04	08	45.98	6.01	4.4 (m_b, NEIC)	OGSI	1
1997	02	24	12	06	43.71	8.47	3.7 (m_b, ISC)	CALF, OGDI, SAOF	3
1997	05	15	00	24	45.23	6.62	3.6 (m_b, ISC)	OGMO, OGMU	2
1997	10	03	15	03	44.32	6.45	3.6 (M_L, NEIC)	CALF, OGCA, STET	3
1997	10	31	04	23	44.26	6.57	4.3 (MED RCMT)	CALF, OGAN, OGCU, OGMO, OGMU, OGSI, OGSR, SAOF	8
1997	11	08	01	56	44.07	7.89	3.6 (m_b, ISC)	CALF, OGCA, OGMO, OGMU, SAOF	5
1999	01	11	03	36	45.10	5.76	3.4 (m_b, ISC)	OGAG, OGBL, OGCU, OGDH, OGLE, OGMB, OGMO, OGMU, OGPC, OGSI, STET	11
2000	06	27	04	07	41.25	9.64	4.3 (MED RCMT)	SMPL	1
2001	02	06	22	28	44.12	8.66	4.2 (ZUR RMT)	MENA, NBOR, NLIB, NROC, OGAN, OGCU, OGDI, OGFH, OGLE, OGMO, STET	11
2001	02	25	18	34	43.49	7.47	4.5 (MED RCMT)	ARBF, MENA, NALS, NBOR, NLIB, NPOR, NROC, OGAN, OGBB, OGCH, OGCU, OGDI, OGFB, OGFH, OGLE, OGMO, OGMU, RUSF, SAOF, STET	20
2001	03	03	01	55	41.29	9.76	4.1 (ZUR RMT)	SMPL	1
2001	11	07	09	40	41.73	9.68	4.5 (MED RCMT)	SMPL	1
2002	02	10	16	21	41.23	9.36	3.7 (m_b, ISC)	SMPL	1
2002	05	16	14	56	42.94	−0.16	3.9 (ZUR RMT)	PYAD, PYAT, PYBE, PYFE, PYLO, PYLS, PYLU, PYP1, PYPE, PYPR	10
2002	05	16	15	14	42.82	−0.15	3.8 (m_b, ISC)	PYAD, PYBE, PYFE, PYLO, PYLS, PYP1, PYPR	7
2002	09	05	20	42	43.05	−0.40	4.1 (M_L, LDG)	PYAD, PYLS, PYPR	3
2002	12	11	20	09	43.04	−0.33	3.7 (IAG)	PYAD, PYAT, PYLS, PYOR, PYPP	5
2002	12	12	17	59	43.11	−0.28	4.0 (IAG)	PYAD, PYAT, PYLI, PYLO, PYLS, PYOR, PYPE, PYPM, PYPP	9
2003	01	21	18	00	43.05	−0.36	4.0 (ZUR RMT)	PYAD, PYAS, PYAT, PYFE, PYLO, PYLS, PYOR, PYPP, PYPM, PYPR	10
2003	02	22	20	41	48.31	6.66	5.0	OGAN, OGBL, OGCH, OGEP, OGLE, OGMA, OGMU, OGSR, STBO, STBR, STDM, STFL, STHE, STMU, STSM, STUF	16
2003	02	26	03	32	42.38	2.12	4.4 (M_L, LDG)	PYAD, PYAT, PYBA, PYFE, PYLI, PYLO, PYLS, PYOR, PYPE, PYPM, PYPR, PYPT	12
2004	02	23	17	31	47.30	6.28	4.5 (ZUR RMT)	OGAN, OGAP, OGCH, OGCU, OGEP, OGFB, OGLE, OGMO, OGMU, OGPO, OGSI, OGSR, OGTB, STBO, STBU, STDM, STHE, STSM	18
2004	09	21	15	48	42.34	2.02	4.4 (IAG)	BRGM, PYAS, PYAT, PYBA, PYBE, PYCA, PYFE, PYFO, PYLI, PYLL, PYLO, PYLS, PYOR, PYPE, PYPR, PYPT	16
2005	09	08	11	27	46.01	6.87	4.6	ANTI, BELV, BRGM, CALF, ESCA, ISOL, NREV, OCCD, OGAN, OGAP, OGBB, OGDH, OGCH, OGDI, OGFB, OGFH, OGFM, OGH1, OGH2, OGH3, OGPC, OGPO, OGSI, OGTB, OGTI, SAOF, STET, STFL, STSM	29

Table 1 continued

YYYY	MM	DD	HH	MIN	Lat.(N)	Lon.(E)	M_w	Stations	NS
2006	09	02	01	21	43.92	7.59	3.6 (m_b, ISC)	ARBF, BELV, CAGN, ESCA, ISOL, MENA, NCAD, NLIB, NROC, NREV, OGCA, OGDI, OGFH, OGGM, OGMO, OGPC, SAOF	17
2006	11	17	18	19	43.08	0.01	4.6 (m_b, ISC)	PYAD, PYAS, PYAT, PYBB, PYBE, PYFE, PYFO, PYLI, PYLO, PYLS, PYLU, PYOR, PYPC, PYPM, PYPP, PYPR, PYPU, PYTB	18
2006	12	16	08	17	42.99	−0.13	4.1 (M_L, LDG)	PYAT, PYBB, PYLO, PYLS, PYOR, PYPC, PYPR, PYPU, PYTB	9
2007	11	15	13	47	43.02	−0.01	4.5 (M_L, LDG)	PYAD, PYAS, PYAT, PYBB, PYBE, PYLO, PYLS, PYOR, PYPC, PYPU, PYTB	11
30 events							3.4 (m_b)–5.3 (M_w)	83 different stations	263

M_w estimates are from Global CMT unless otherwise stated. NS is number of records used from that event

Other regions contribute few records and therefore they are not examined separately.

According to the classifications given on the RAP website, 178 of the selected records are from rock stations, 75 are from soil stations and 10 are from borehole stations. Note that, although κs were estimated from borehole records they were not used to derive the following models. Possible dependence of κ on the local site conditions is investigated in Sect. 5. A number of stations have recorded multiple earthquakes, which allows a station-specific κ model to be established. Specifically, in Sect. 5 we develop such models for 11 stations that have recorded more than five earthquakes amongst those selected: OGAN (6 records), OGMO (8), OGMU (7), OGSI (6), PYAD (9), PYAT (9), PYFE (7), PYLO (9), PYLS (11), PYOR (8) and PYPR (8).

3. Method Used to Estimate κ

In this study the classic method of estimating κ developed by Anderson and Hough (1984) is used. It is slightly modified [as done by Hough *et al.*, (1988) for a comparable dataset] due to the use of high-quality digital records from small events rather than analogue records from moderate and large earthquakes as used by Anderson and Hough (1984). Each component of a triaxial record is processed individually. The first step is to remove the mean and plot the acceleration time-history. Time-histories that are too noisy or have other problems are rejected. Next, the pre-event, P-wave and S-wave portions of the time-history are selected by eye. Then the Fourier amplitude acceleration spectra of each of these three portions are computed and plotted on the same graph with a logarithmic y-axis (amplitude) and a linear x-axis (frequency). Based on the S-wave spectra two frequencies are selected by visual inspection: f_E, the start of the linear downward trend in the acceleration S-wave spectrum, and f_X, the end of the linear downward trend or when the S-wave spectrum approaches the noise spectrum (i.e. when the signal-to-noise ratio becomes too small for the spectral amplitudes to be reliable). Figure 2 shows an example of a spectra with a clear high-frequency linear trend and low noise levels and the f_E and f_X frequencies chosen for this record by one of the analysts. We find that f_E is generally around 3 Hz but with a large scatter [within the 2–12 Hz range used by Anderson and Hough (1984)]. Thanks to the high resolution and low noise levels of the selected records f_X is generally in the range 20–50 Hz. The final step in the procedure is to fit, using standard least-squares regression, a line fitting the acceleration spectrum between f_E and f_X, from whose slope κ is given by $\kappa = -\lambda/\pi$ where λ is the slope of the best-fit line. Generally there is a sufficient frequency range between f_E and f_X to give a robust estimate of κ.

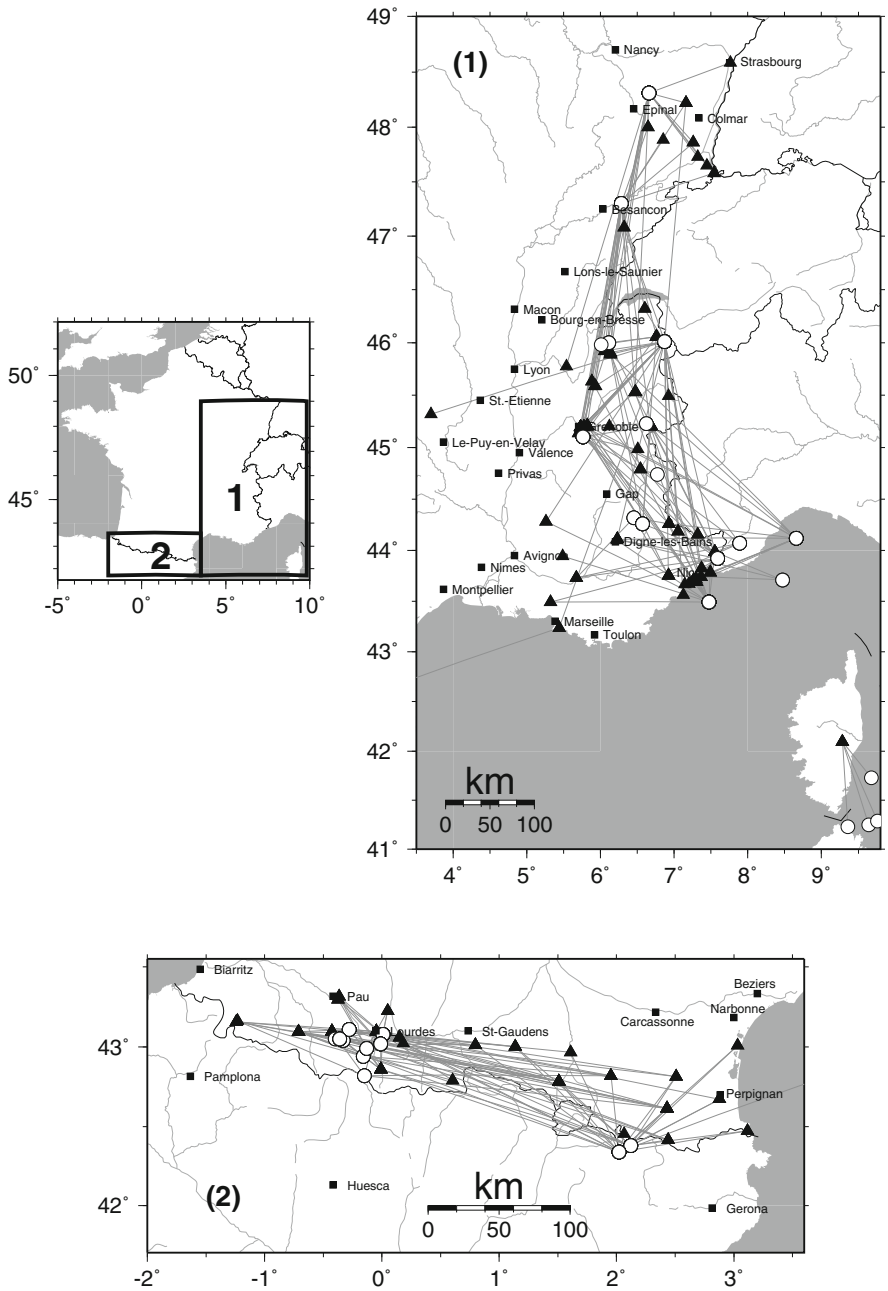

Figure 1
Earthquake (*circles*) and station (*triangles*) locations and travel paths (*lines*) of the records used for this study. *1* Alps and Côte d'Azur (southern part of map) and *2* Pyrenees

A non-automatic procedure for estimating κ was adopted because we noted that the frequency, f_E, at which the acceleration spectral amplitudes show a decline varied significantly from record to record and therefore assuming a constant f_E, such as has been done in some previous studies, could lead to biased estimates for κ. Similarly, due to varying signal-to-noise ratios (visually inspected), f_X shows large variations and therefore it was not possible to use a constant value for all records. Since the procedure followed here is non-automatic, it is quite time-consuming and also subjective because analysts can have

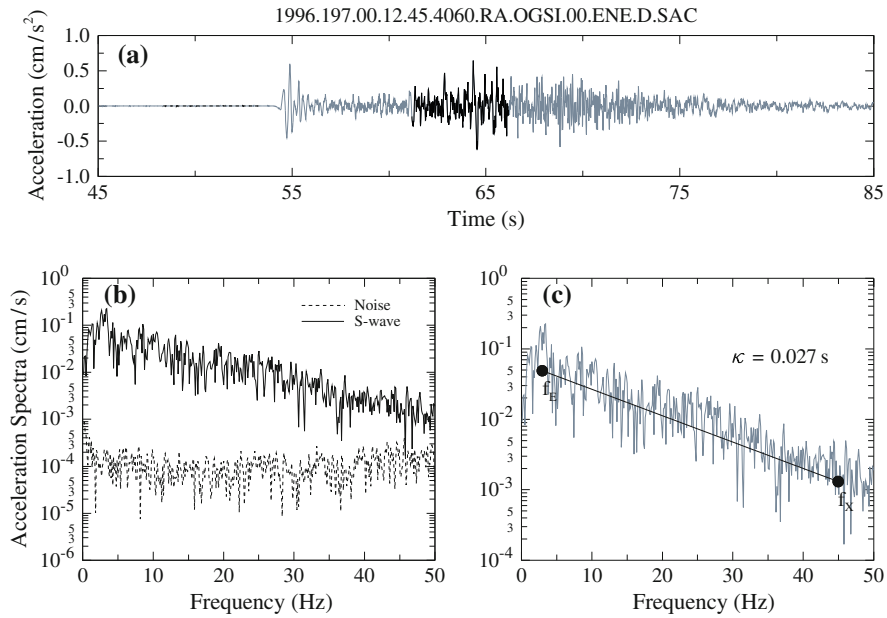

Figure 2
Example of direct shear-wave and noise spectra computed from a record that shows a clear high-frequency linear trend. Also shown are the intervals used to estimate the pre-event noise and the direct shear-wave spectra (black parts of acceleration time-history) and the frequencies f_E and f_X chosen by one of the analysts (the other analysts chose similar f_E and f_X for records such as this)

different views on the selection of the pre-event, P-wave and S-wave portions of the record and on the selection of f_E and f_X, which can lead to some variations in κ between analysts. We found that differences in picking of the pre-event, P-wave and S-wave portions did not significantly affect the κs obtained.

A semi-automatic procedure to choose the intervals used to compute the direct shear-wave spectra and noise spectra was also applied. Since both P- and S-wave arrival times had been previously picked, time windows of 5 s for the pre-event noise and direct S-wave were used to compute the Fourier spectra. Various lengths of time windows from 1 to 10 s were also tested with similar results, so a standard length of 5 s was finally chosen. The time series were processed using a Hanning taper of 5%. The resulting Fourier spectra were then smoothed by a Konno and Ohmachi (1998) filter (filter bandwidth of 40), and only data having a signal-to-noise ratio greater than three were used to compute κ. The values of f_X and f_E used to compute κ in this procedure were chosen by the analyst, as in the completely manual approach described above. In the next section we present the approach we took to quantify the subjectivity and precision of the obtained κs.

In the absence of the high-frequency decay quantified here by κ Fourier amplitude spectra should be flat above the corner frequency, f_c, of the source. When fitting the best-fit lines to determine κ it is necessary that f_E (the frequency chosen as the start of the best-fit line) is greater than f_c otherwise the κ estimates can be biased. When using strong-motion data from moderate and large earthquakes ($M_w \geq 5.5$) as done by Anderson and Hough (1984) f_c is generally lower than 1 Hz hence bias in κ due to f_c is not a problem. However, in this study where we are using data from earthquakes with $3.4 \leq M \leq 5.3$ f_c is generally between 1 and 6 Hz, using Fig. 8 of Drouet *et al.* (2008) showing the relation between magnitude and f_c. The f_E values are selected here to be above f_c based on visual inspection (Figs. 2, 3) and, therefore, most best-fit lines will be minimally affected by f_c, especially since f_X (the frequency up to which the line is fitted) is usually greater than 30 Hz.

Site amplification curves, relative to reference sites displaying little amplification, for some of the stations considered here are provided by Drouet

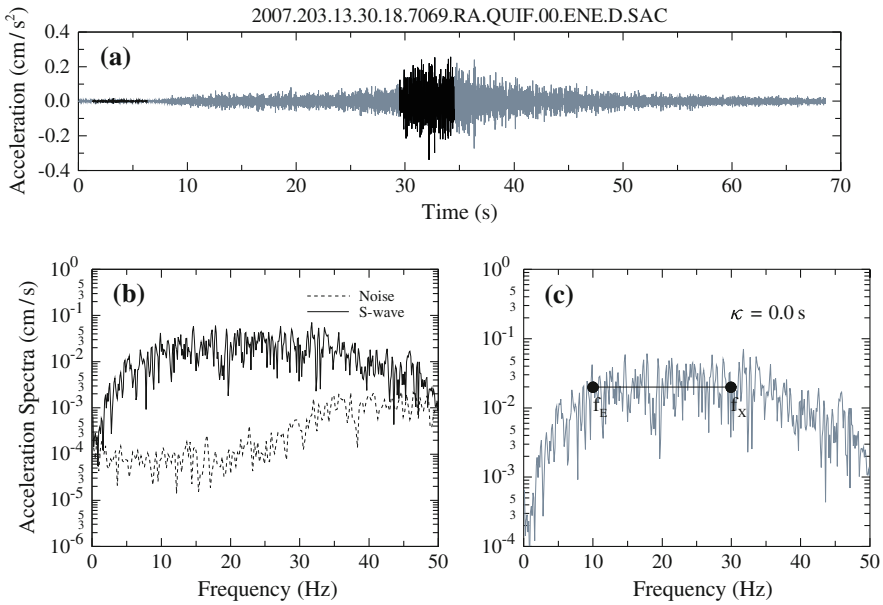

Figure 3
Example of direct shear-wave and noise spectra computed from a record used in the analysis that shows a high-frequency site effect seen on all records from this station (and hence it is difficult to estimate a reliable κ from this record). Also shown are the intervals used to estimate the pre-event noise and the direct shear-wave spectra (black parts of acceleration time-history) and the frequencies f_E and f_X chosen by one of the analysts (f_E and f_X for records such as this varied between analysts)

et al. (2008). Some of these curves show peaks in the site amplifications at high frequencies where they could complicate the estimation of κ (e.g. >5 Hz), e.g. PYAD and PYBA. Although not investigated by Drouet *et al*. (2008), records from QUIF also show a high-frequency site effect (see Fig. 3). In our analysis we attempted to compensate for the peak in the Fourier amplitude spectra from such stations to avoid biasing the obtained κs (as done by Anderson and Hough (1984) for Santa Felicia Dam, with a similar high-frequency amplification). The relative site amplification curves for 49 stations provided by Drouet *et al*. (2008) could be used to correct the observed spectra as done by Margaris and Boore (1998), for example, but this has not been attempted for simplicity, and in order to be consistent between all records, even those from stations not analyzed by Drouet *et al*. (2008). Parolai and Bindi (2004) conduct simulations assuming a 1D single sedimentary layer overlaying a bedrock half-space and earthquakes with $2 \leq M_w \leq 6$ to examine the effect of local site amplification on κ estimates. They find that in the presence of strong site amplifications at frequencies greater than 4 Hz, it is necessary to fit the best-fit line to determine κ over a wide frequency band (e.g. 10–34 Hz) in order to obtain accurate κs. Thanks to the high resolution (24 bits) and low noise levels on the digital accelerograms used in this study we are generally able to extend the fitting of the best-fit lines to 30 Hz or higher. Therefore, it is likely that most κ estimates found here are not biased by high-frequency site effects. However, the combination of high-frequency site effects and higher noise levels at some RAP stations means that some κ values obtained in this study may be too high (see Sect. 5).

3.1. *Variability in κ Estimates*

The first three authors of this article independently processed (the first two using the non-automatic procedure and the third the semi-automatic technique) the 263 records and their estimated κs were compared. It was found that for most records the estimated κs of the three analysts were similar (within 10–20% of one another) but for some records with no clear linear amplitude dependence on frequency the measured κs vary greatly (up to 50%). After discussion, some of these large differences were reduced by one or two

analysts reprocessing the problem records. However, there remains a subjective aspect to the estimation of κ. Therefore, due to the variability in κ among individual accelerograms, we believe that robust estimates of κ at seismic stations should be based on a large number of individual observations. Therefore, in this study we only seek conclusions based on many records. Note that, as discussed above, if the best-fit lines are estimated over a frequency band affected by high-frequency site amplifications or high corner frequencies, κ estimates could be biased either upwards or downwards. In this situation, whatever method is used to average the estimates from each analyst the κs obtained will not be correct. As stated above we do not think that this is the situation for the vast majority of the records we analyzed.

By analyzing the three κ estimates from a single record it was found that the error in the measurement of an individual κ were multiplicative rather than additive, i.e. κ estimates from each analyst were higher or lower than the average κ by a certain percentage (e.g. 20%) rather than by an absolute amount (e.g. 0.005 s). Assuming multiplicative errors also has the benefit of excluding the possibility of predicting negative κs. Therefore, the logarithms of the six κ estimates for an individual record (from three analysts and for the two horizontal components) were computed and the mean and standard deviations computed from these six logarithms were used in the subsequent analysis. By averaging κs for both horizontal components we make the assumption that κ is the same for both components and hence it is independent of the azimuth of the incoming waves. The mean κs and associated standard deviations were then used to undertake weighted regression analysis using diagonal weighting matrices derived from the inverse variances of each κ estimate (e.g. Draper and Smith, 1998). Since the variances are derived from the logarithms of the κs but the regression was performed on the untransformed κs (to be consistent with previous studies), the weighting matrices are slightly incorrect with respect to the regression performed, but we do not believe that this significantly affects the results. A traditional, non-weighted least squares regression was also computed in order to see the effect of the uncertainty measured on the κ values. Both regressions are quite similar. The results of these regression analyses are reported below.

3.2. κ Estimates from Vertical Components

κ was computed for the three components of ground motion but only the horizontal components were used to develop the κ models. Figure 4 shows the relation between the κ values computed using the horizontal and vertical components. The error bar for each measurement has also been plotted. This figure shows that vertical estimates are slightly smaller than the horizontal ones but, in general, the estimates are similar. In absence of three-component stations, κ values obtained from vertical components may be helpful for a first estimate of this parameter, although a slight adjustment of κs from vertical components could be required.

4. Distance Dependence

The first-order model that is often fitted to κ estimates is: $\kappa = \kappa_0 + m_\kappa\, r_{\text{epi}}$, where r_{epi} is epicentral distance and κ_0 and m_κ are constants (e.g. Anderson and Hough, 1984). κ_0 is believed to be station-dependent and related to the near-surface attenuation in the top couple of kilometers under the site whereas m_κ is believed to be region-dependent and related to the regional attenuation. As mentioned

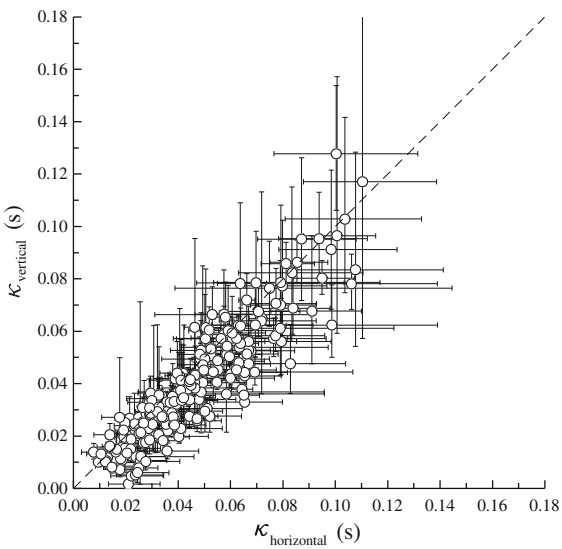

Figure 4
Comparison of κ values computed from vertical and horizontal components. ± 1 standard deviation bars are also plotted. The *dashed line* represents the 1:1 relation

above in this study we have used the estimated standard deviations of each κ value to apply weighted regression analysis to find κ_0 and m_κ for our data. The results from non-weighted regression are also shown in the legend of the corresponding figures for completeness.

As a first step regression analysis is performed for all surface records (263 records) using the form: $\kappa = \kappa_{0,\mathrm{rock}} S_{\mathrm{rock}} + \kappa_{0,\mathrm{soil}} S_{\mathrm{soil}} + m_\kappa\ r_{\mathrm{epi}}$, where $S_{\mathrm{rock}} = 1$ for rock stations and 0 otherwise and $S_{\mathrm{soil}} = 1$ for soil stations and 0 otherwise. By using this functional form we allow near-surface attenuation at rock stations to be different from that at soil stations but we assume that the regional attenuation is the same since a common m_κ is used for rock and soil sites. The estimated κs with respect to r_{epi} and site class are shown in Fig. 5 along with the fitted lines. The equations of the best-fit lines are:

$$\begin{aligned} \kappa_{\mathrm{soil}} &= 0.0270 + 0.000175 r_{\mathrm{epi}} \\ \kappa_{\mathrm{rock}} &= 0.0207 + 0.000175 r_{\mathrm{epi}}. \end{aligned} \tag{1}$$

Note that if these models are used in SMSIM (Boore, 2005), for example, then it is not also necessary to apply Q attenuation since this is already included in these κ models. However, it is standard practice when using SMSIM to use only the κ_0 terms and model the regional attenuation through a Q model.

Hough *et al.* (1988) present equations for estimating a two-layer Q model from κ_0 and m_κ values. Their approach has not been applied here because the values found using this method assume that Q is independent of frequency, which has not previously been found in France (e.g. Campillo *et al.*, 1985; Drouet *et al.*, 2008). The Q tomography technique of Hough and Anderson (1988) has not been attempted since the distribution of data with respect to distance is insufficient and, in addition, there is not enough resampling of travel paths.

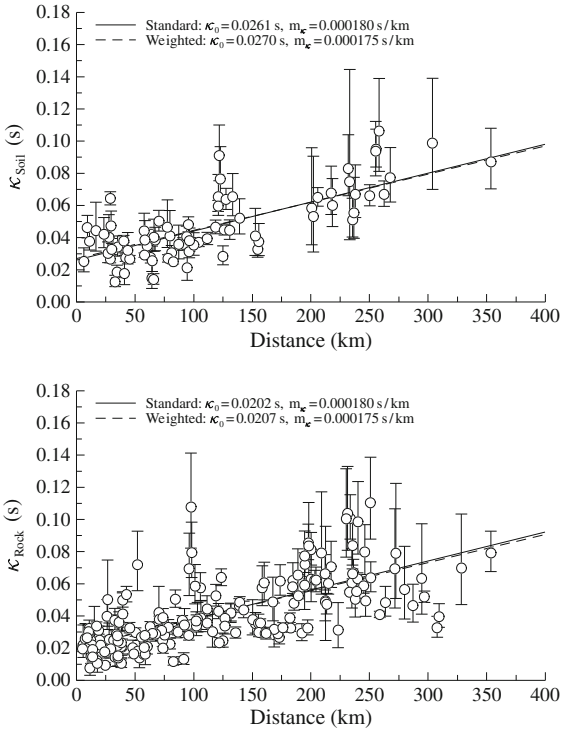

Figure 5
Distance dependence of κ for all stations for soil and rock conditions. The *vertical lines* represent the standard deviation of six independent measurements of κ (three estimates, two horizontal components). Results for κ_0 and m_κ from standard (*solid line*) and weighted (*dashed line*) least squares regressions are shown in the legend of each plot

5. Regional Dependence

There are sufficient records from the Pyrenees (109 records), the Alps (88 records) and the Côte d'Azur (50 records) to derive individual best-fit equations for these regions. Figure 6 shows the κ values for these three regions for both soil and rock conditions. The regional m_κ values are relatively close to each other. However, we find that the Pyrenees area has slightly lower attenuation than the Alps, and both are less attenuating than the Côte d'Azur. These results are in agreement with regional attenuation studies in France using the isoseismal distribution from historical earthquakes (e.g. Baumont and Scotti, 2006) and previous Q estimates by Drouet *et al.* (2008), who find lower Q values for the Alps (322), i.e. faster attenuation, than for the Pyrenees (376).

These differences between regions are also observed on the κ_0 values for stations located on rock but the stations in the Alps show a larger attenuation than the other two regions for stations located on soil.

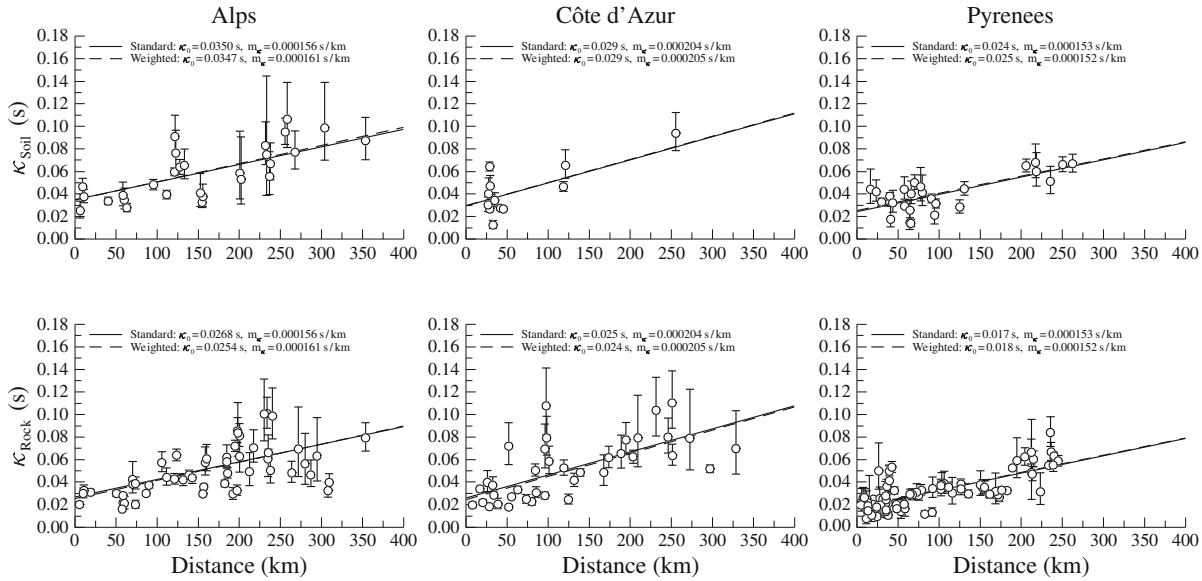

Figure 6
Distance dependence of κ values for three regions in mainland France. The *top* plots present the results for stations located on soil. The *bottom* plots show the results for stations located on rock

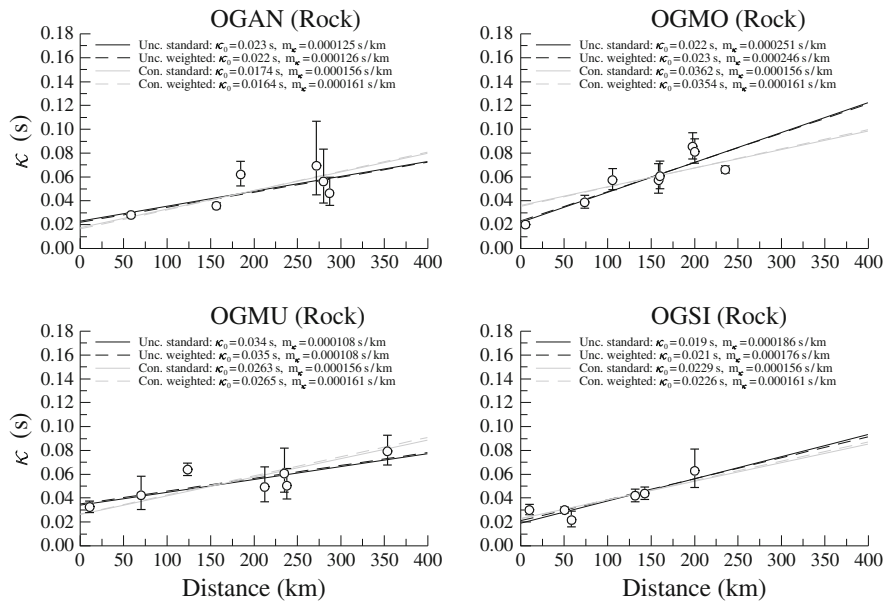

Figure 7
κ estimates and their ± 1 standard deviations for stations located in the Alps. Also shown are the fitted linear relations. Four best-fit lines were fitted for each station: two (using standard and weighted regression) in which m_κ was allowed to vary (*black*) and two (using standard and weighted regression) in which m_κ was constrained to the value from the regional analysis shown in Fig. 6 (*grey*)

This may be explained by the fact that some of the stations are located in the sedimentary Grenoble basin where the deep soil layer could lead to large attenuation.

Figures 7 and 8 show κ estimates and fitted linear relations for 11 stations located in the Alps and the Pyrenees. Two sets of fits were made: one in which the slope (m_κ) and the intercept (κ_0) were

unconstrained and one in which m_κ was fixed to the value obtained from the regional analysis reported in Fig. 6 and a corresponding κ_0 found. Considering the unconstrained fits, for stations located in the Alps, all of which are sited on rock, m_κ shows modest variations of about 50% around the (m_κ) estimated for this region (Fig. 6), whereas in the Pyrenees (Fig. 8), the variability of $m_{\kappa\kappa}$ is larger. Concerning κ_0 the values for stations in the Alps (Fig. 7) present similar values to those obtained for the whole region (Fig. 6). An interesting exception is station OGMU whose κ_0 value for the unconstrained fits is quite close to the soil estimate in this region. This could be due to a site effect at about 10 Hz for this station (Drouet *et al.*,

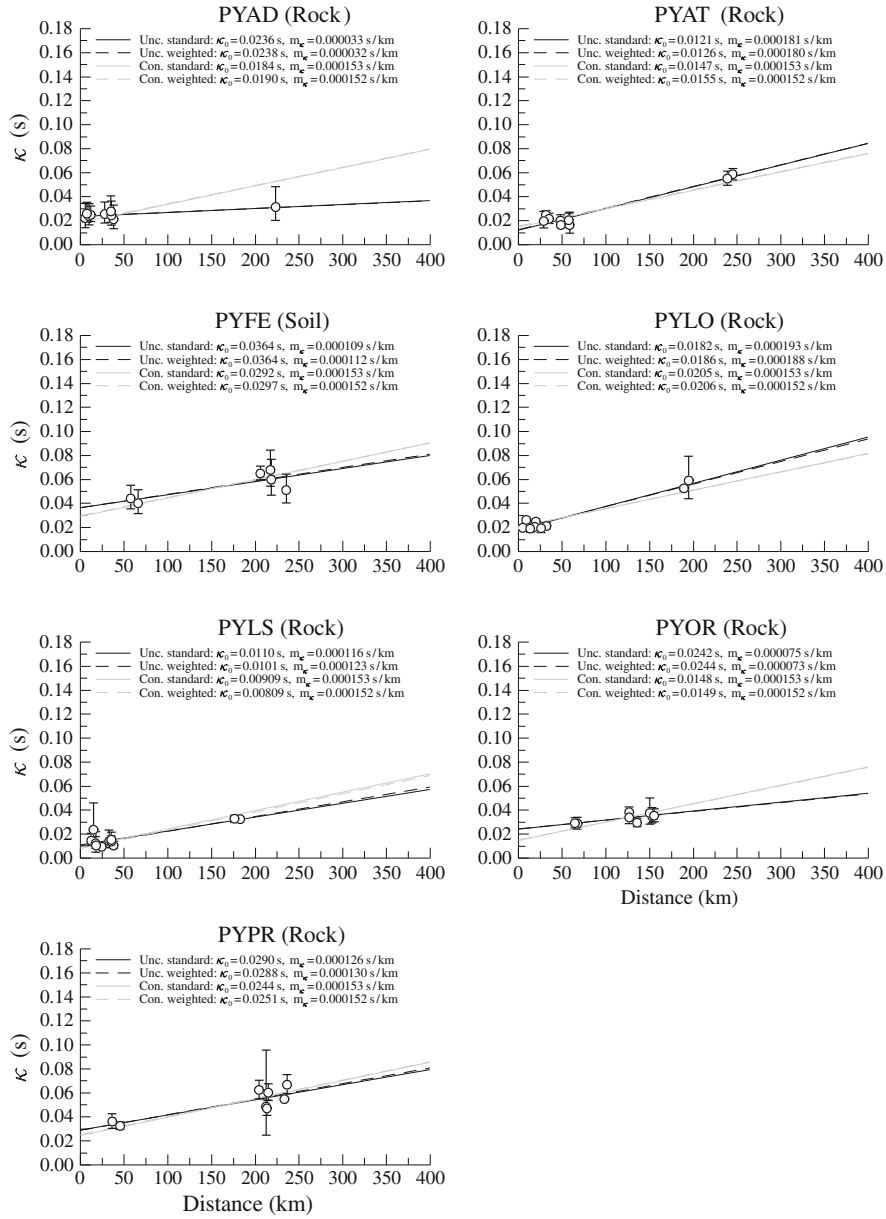

Figure 8
κ estimates and their ± 1 standard deviations for stations located in the Pyrenees. Also shown are the fitted linear relations. Four best-fit lines were fitted for each station: two (using standard and weighted regression) in which m_κ was allowed to vary (*black*) and two (using standard and weighted regression) in which m_κ was constrained to the value from the regional analysis shown in Fig. 6 (*grey*)

2008), which could bias upwards the estimates of κ (Parolai and Bindi, 2004). Stations located in the Pyrenees present a larger variation of κ_0 with respect to the value computed for the whole region. This variability may come from structural differences beneath each station or perhaps from statistical variations in small sample sizes. Given the variation in the distribution of records with respect to distance between stations, the fits in which m_κ is constrained to its regional value are probably more reliable. These fits suggest that κ_0 for some Pyrenean rock stations (e.g. PYAT, PYLS and PYOR) is lower than at the average rock station.

6. Conclusions

In this article we have estimated the high-frequency attenuation parameter κ (Anderson and Hough, 1984) from 263 high-quality triaxial accelerograms from the French RAP strong-motion network. Furthermore, we have investigated the dependence of κ on distance, region and site conditions to develop simple κ models for use in seismic hazard assessment for mainland France. We have found that the three studied regions (the Pyrenees, the Alps and the Côtes-d'Azur) present different yet relatively similar dependency of κ on epicentral distance. The influence of local geology is slight yet noticeable.

The values obtained here are reasonably consistent with, although larger than (meaning higher attenuation), the 0.015 and 0.0125 s values obtained for Switzerland by Bay *et al*. (2003) and Bay *et al*. 2005, respectively, and the 0.012 s value for the western Alps found by Morasca *et al*. (2006), using a different technique. This could be attributed to more competent rock (higher shear-wave velocities) in Switzerland than in France. In contrast our average $\kappa\kappa\kappa_0$ is lower than the 0.05 s value found by Malagnini *et al*. (2000) for central Europe (mainly Germany).

Based on these results, in terms of near-surface attenuation it seems that mainland France lies between WNA (where κ has been found to be around 0.04 for rock sites) and ENA (where κ has been found to be much lower, 0.006 is a commonly used value). Similarly Campillo *et al*. (1985) concluded that their Q model situates France between ENA and WNA in terms of regional attenuation. This seems reasonable with respect to the seismotectonics of France (mainly a stable continental region but with areas of active tectonics, the Pyrenees and the Alps) and its geology (quite hard bedrock sites). Therefore, seismic hazard assessments for France could be conducted by adjusting κ contributions to GMPEs from active regions downwards or κ for GMPEs from stable continental regions upwards to the intermediate κ values we estimated.

Acknowledgments

This study was funded by BRGM research and public service projects and a grant from the Réseau Accélérometrique Permanent (RAP) of France. The strong-motion networks in France are operated by various organizations (see the RAP website), under the aegis of the RAP. The RAP data centre is based at Laboratoire de Géophysique Interne et de Tectonophysique, Grenoble. We are very grateful to the personnel of these organizations for operating the stations and providing us with the data, without which this study would have been impossible. Finally, we thank Stéphane Drouet, Glenn Biasi and David Boore for careful and detailed reviews of earlier versions of this article and Stéphane Drouet for his GMT script to draw maps of epicentral and station locations and travel paths.

References

Anderson, J. G. and Hough, S. E. (1984), *A model for the shape of the Fourier amplitude spectrum of acceleration at high frequencies*, Bull. Seismol. Soc. Am. *74*(5), 1969–1993

Atkinson, G. M. (2008), *Ground-motion prediction equations for eastern North America from a referenced empirical approach: Implications for epistemic uncertainty*, Bull. Seismol. Soc. Am. *98*(3), 1304–1318. doi:10.1785/0120070199.

Atkinson, G. M. and Boore, D. M. (2006), *Earthquake ground-motion prediction equations for eastern North America*. Bull. Seismol. Soc. Am. *96*(6), 2181–2205. doi:10.1785/0120050245.

Baumont, D. and Scotti, O. *On the impact of the binning strategy on macroseismic magnitude-depth-I_0 estimates*. In *Proceedings of First European Conference on Earthquake Engineering and Seismology (a joint event of the 13th ECEE & 30th General Assembly of the ESC)*, Sep 2006. Abstract CS2-625.

Bay, F., Fäh, D., Malagnini, L. and Giardini, D. (2003), *Spectral shear-wave ground-motion scaling in Switzerland*, Bull. Seismol. Soc. Am. *93*(1), 414–429.

Bay, F., Wiemer, S., Fäh, D. and Giardini, D. (2005), *Predictive ground motion scaling in Switzerland: Best estimates and uncertainties*. J. Seismol. *9*, 223–240.

Bommer, J. J., Stafford, P. J., Alarcón, J. E. and Akkar, S. (2007), *The influence of magnitude range on empirical ground-motion prediction*, Bull. Seismol. Soc. Am. *97*(6), 2152–2170. doi:10.1785/0120070081.

Boore, D. M. *SMSIM—Fortran programs for simulating ground motions from earthquakes: Version 2.3—A revision of OFR 96-80-A. Open-File Report 00-509*, United States Geological Survey, Aug 2005. Modified version, describing the program as of 15 August 2005 (Version 2.30).

Campbell, K. W. (2003), *Prediction of strong ground motion using the hybrid empirical method and its use in the development of ground-motion (attenuation) relations in eastern North America*, Bull. Seismol. Soc. Am. *93*(3), 1012–1033.

Campillo, M., Plantet, J. -L. and Bouchon, M. (1985), *Frequency-dependent attenuation in the crust beneath central France from Lg waves: Data analysis and numerical modeling*, Bull. Seismol. Soc. Am. *75*(5), 1395–1411.

Campillo, M., Feignier, B., Bouchon, M. and Béthoux, N. (1993), *Attenuation of crustal waves across the Alpine Range*, J. Geophys. Res. *98*(B2), 1987–1996.

Cotton, F., Scherbaum, F., Bommer, J. J. and Bungum, H. (2006), *Criteria for selecting and adjusting ground-motion models for specific target regions: Application to central Europe and rock sites*, J. Seismol. *10*(2), 137–156. doi:10.1007/s10950-005-9006-7.

Cotton, F., Pousse, G., Bonilla, F., and Scherbaum F. (2008), *On the discrepancy of recent European ground-motion observations and predictions from empirical models: Analysis of KiK-net accelerometric data and point-sources stochastic simulations*, Bull. Seismol. Soc. Am. *98*(5), 2244–2261. doi:10.1785/0120060084.

Douglas, J., Bungum, H. and Scherbaum, F. (2006), *Ground-motion prediction equations for southern Spain and southern Norway obtained using the composite model perspective*, J. Earthq. Eng. *10*(1), 33–72.

Douglas, J., Gehl, P., Bonilla, L. B., Scotti, O., Régnier, J., Duval, A. -M. and Bertrand, E. (2009), *Making the most of available site information for empirical ground-motion prediction*, Bull. Seismol. Soc. Am. *99*(3), 1502–1520. doi:10.1785/0120080075.

Draper, N. R. and Smith, H. (1998), *Applied regression analysis*. (3rd edn. Wiley, New York).

Drouet, S., Souriau, A. and Cotton, F. (2005), *Attenuation, seismic moments, and site effects for weak-motion events: Application to the Pyrenees*. Bull. Seismol. Soc. Am. *95*(5), 1731–1748. doi:10.1785/0120040105.

Drouet, S., Chevrot, S., Cotton, F. and Souriau, A. (2008), *Simultaneous inversion of source spectra, attenuation parameters, and site responses: Application to the data of the French Accelerometric Network*, Bull. Seismol. Soc. Am. *98*(1), 198–219. doi:10.1785/0120060215.

Hough S.E., Anderson J.G. (1988) High-frequency spectra observed at Anza, California: Implications for *Q* structure. Bulletin of the Seismological Society of America, 78(2):692–707

Hough, S. E., Anderson, J. G., Brune, J., Vernon, III F., Berger, J., Fletcher, J., Haar, L., Hanks, T. and Baker, L. (1988), *Attenuation near Anza, California*, Bull. Seismol. Soc. Am. *78*(2), 672–691.

Konno, K. and Ohmachi, T. (1998), *Ground-motion characteristics estimated from spectral ratio between horizontal and vertical components of microtremor*, Bull. Seismol. Soc. Am. *88*(1), 228–241.

Malagnini, L., Herrmann, R. B. and Koch, K. (2000), *Regional ground-motion scaling in central Europe*, Bull. Seismol. Soc. Am. *90*(4), 1052–1061.

Margaris, B. N. and Boore, D. M. (1998), *Determination of $\Delta\sigma$ and κ_0 from response spectra of large earthquakes in Greece*. Bull. Seismol. Soc. Am. *88*(1), 170–182.

Morasca, P., Malagnini, L., Akinci, A., Spallarossa, D. and Herrmann, R. B. (2006), *Ground-motion scaling in the western Alps*, J. Seismol. *10*(3), 315–333. doi:10.1007/s10950-006-9019-x.

Papageorgiou, A. S. and Aki, K. (1983), *A specific barrier model for the quantitative description of inhomogeneous faulting and the prediction of strong ground motion. Part I. Description of the model*, Bull. Seismol. Soc. Am. *73*(3), 693–702

Parolai, S. and Bindi, D. (2004), *Influence of soil-layer properties on κ evaluation*, Bull. Seismol. Soc. Am. *94*(1), 349–356.

Péquegnat, C., Guéguen, P., Hatzfeld, D. and Langlais, M. (2008), *The French Accelerometric Network (RAP) and National Data Centre (RAP-NDC)*, Seismol. Res. Lett. *79*(1), 79–89.

Silva, W., Darragh, R., Gregor, N., Martin, G., Abrahamson, N. and Kircher, C. (1998), *Reassessment of site coefficients and near-fault factors for building code provisions*. Technical Report Program Element II: 98-HQ-GR-1010, Pacific Engineering and Analysis, El Cerrito, USA

Tsai, C-C. P. and Chen, K. -C. (2000), *A model for the high-cut process of strong-motion accelerations in terms of distance, magnitude, and site condition: An example from the SMART 1 array, Lotung, Taiwan*, Bull. Seismol. Soc. Am. *90*(6), 1535–1542.

(Received May 27, 2009, revised January 7, 2010, accepted February 4, 2010)

5 ANNEXE 2: ON THE USE OF SAENGER'S FINITE DIFFERENCE STENCIL TO MODEL 2D P-SV NONLINEAR BASIN RESPONSE: APPLICATION TO NICE, FRANCE

On the use of Saenger's finite difference stencil to model 2D P-SV nonlinear basin response: application to Nice, France

GELIS, Céline, BONILLA, Luis Fabian
BERSSIN/IRSN. BP 17. 92262 Fontenay-aux-roses cedex. France

REGNIER, Julie, BERTRAND, Etienne, DUVAL, Anne-Marie
CETE Mediterranée. Equipe « risque sismique ». Laboratoire de Nice. 56 Bd Stalingrad. 06359 Nice cedex 4. France

Abstract

In this study we present 1D and 2D linear and nonlinear wave propagation simulations in the Nice basin up to 10 Hz. In particular, we compute the basin response for different angles of incidence of the incoming wavefield. The numerical computations show that the impedance contrast between the sediments and surrounding bedrock produces a strong amplification regardless of the basin geometry. However, the basin geometry produces amplification values between 4 and 5 times higher than the ones computed with the 1D model for a broadband frequency range. These results agree with observed weak motion data in the region. Numerical nonlinear site response shows a strong dependency of the amplification factor to the angle of incidence of the incoming wavefield. This suggests that a 2D and 3D geometry should be taken into account for a more accurate estimation of the basin response.

Introduction

In previous years there have been numerous studies about wave propagation in complex media (i.e. [1], [2], [3]). Most of these studies concentrate their attention on large basins, such as those in the USA, Japan, and New Zealand among others. However, other regions equally prone to earthquake hazards are located on small basins where a large number of people live and an important economic activity may also be present. This is the case for some European cities, for example the Nice basin.

Throughout the world, numerous examples have proven the importance of site effects in basins. The basin response depends on the site geometry, impedance

contrast, material elastic and dynamic properties, and on the strength of the input solicitation that may lead to strong nonlinear effects. Numerical modeling is a useful tool to understand the role and the influence of these different parameters governing site effects. In this study, we focus on the Nice basin and perform a comparison regarding the influence of the 2D basin geometry with respect to 1D approximations. At last, we compare our results with real data.

Numerical scheme for simulating 2D P-SV seismic wave propagation

Saenger et al.'s stencil [4]

We use the [4] finite difference (FD) stencil to model 2D P-SV wave propagation. This stencil allows computing all components of the stress-strain tensor in one point of the numerical mesh, which simplifies the implementation of the computation of nonlinear soil rheologies as it is done in finite element schemes (figure 1). Moreover, this stencil avoids using twice physical parameters, such as density and shear modulus, in the numerical mesh (figure 1). Thanks to these stencil properties, wave propagation in heterogeneous linear and nonlinear media is efficiently modeled. Furthermore, the free surface is easily introduced by zeroing Lamé parameters above the free surface and surface waves can be modeled more accurately ([5]) than with traditional staggered-grid methods ([6]). In this study, we introduce attenuation for all linear simulations by using the method of [7]. The strain-stress relation, governing the non linear behavior modeling and used at each time step, is detailed in the next section.

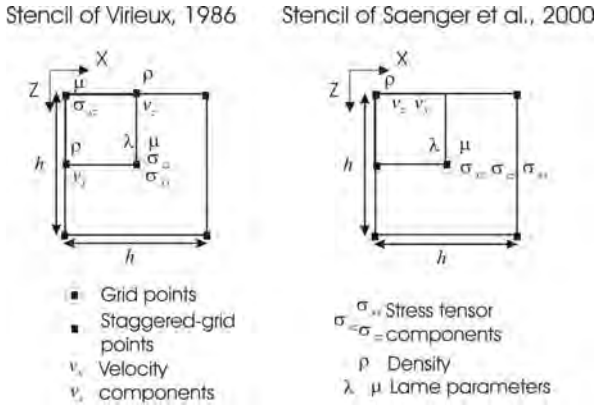

Figure 1: Numerical mesh and stencil for the FD staggered-grid of [6] and of [7]

Nonlinear stress-strain rheology

The multishear mechanism model ([8]) is a plane strain formulation to simulate pore pressure generation in sands under cyclic loading and undrained conditions. [9] and [10] modified the model to account for the cyclic mobility and dilatancy of sands. However, in its basic form, this formulation models soil nonlinearity in dry conditions, which is the case here. The multiple mechanism model relates the stress σ and strain ε through the following incremental equation ([9], [10]),

$$\{d\sigma'\} = [D] (\{d\varepsilon\} - \{d\varepsilon_p\}) \quad (1)$$

where the curly brackets represent the vector notation; $\{\varepsilon_p\}$ is the volumetric strain produced by the pore pressure, and [D] is the tangential stiffness matrix. This matrix is composed by the volumetric and shear mechanisms, which are represented by the bulk and tangential shear moduli, respectively. The latter is idealized as a collection of I springs separated by $\Delta\theta = \pi / I$ (Figure 2). Each spring follows the hyperbolic stress-strain model ([11]) and the generalized Masing rules for the hysteresis process. For more details on the model the reader may see the papers by [9] and [10].

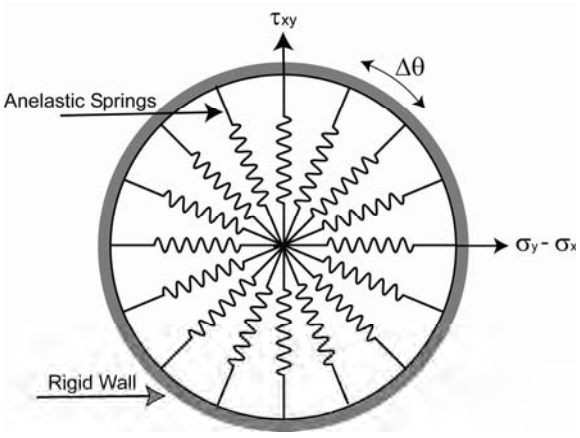

Figure 2: Schematic figure for the multiple simple shear mechanism. The plane strain is the combination of pure shear (vertical axis) and shear by compression (horizontal axis) (after [8]).

Application to Nice, France

The city of Nice is located in the south eastern of France, between the Alps and the Mediterranean Sea. The regional seismicity is moderate but not negligible.

Five RAP (French Permanent Accelerometric Network) stations are located in the city, four in the quaternary sedimentary basin of Nice (stations NLIB, NPOR, NROC, NALS) and one at "rock" (station NBOR). Experimental measurements of site effects ([12]), who used microtremors and earthquakes recordings, clearly indicated that site amplification occurs in Nice. In addition, large amounts of geotechnical data are available in the whole city and a 3D geotechnical model and soil nonlinear dynamic parameters have been produced ([13]). Hence, Nice is a natural choice to study site effects using different numerical techniques and their comparison with observed data.

Using the 3D geotechnical model, 1D and 2D numerical simulations have been performed along the profile containing station NLIB. The model size is 125 m deep and 2,2 km length. The minimum and maximum shear wave velocity is 180 and 1000 m/s in the sediments (obtained from SPT-Vs correlations) and bedrock, respectively. In the absence of information regarding P-wave velocity, we assumed a Poisson's coefficient of 0.4. The quality factor values Q_P and Q_S are estimated as one tenth of the P- and S-wave velocities, respectively. The computations were carried out up to 10 Hz and the numerical spatial and time steps were 0.5 m and 1.0^{-4} s. For the source, we used a synthetic accelerogram simulating a M6 earthquake located at 8 km hypocentral distance and having a PGA of 0.2g. Note that the rock reference station, NBOR, is not contained in the 2D profile. Thus, in order to have a reference in our numerical model, we extended the model laterally so that rock outcrop motions can be obtained.

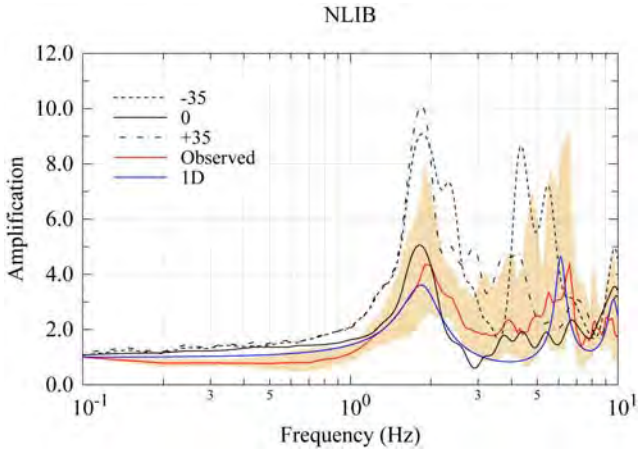

Figure 3: Observed (red line and dashed area) and computed (black lines) amplification transfer function for RAP site NLIB.

Figure 3 shows the amplification transfer function for station NLIB. This result was obtained computing traditional spectral ratios (NLIB/NBOR) for recorded

earthquakes (East-West horizontal components). The red line and the dashed area represent the mean amplification and its 68% confidence limits, respectively. The mean amplification factor is around 4 and two clear resonance frequencies are identified at 2 and 6-7 Hz, respectively. Furthermore, figure 3 shows the results for the 1D and 2D simulations at NLIB. Both 1D and 2D models agree with the observations in spite of having different reference station. However, for inclined incident wavefield (35° with respect to horizontal direction, coming from the left (+35°) and from the right (-35°) in the basin, respectively), the amplification is quite different from vertically incident wavefield.

2D P-SV linear modeling

Vertical incidence

Figure 4 shows the amplification of the transfer function for 1D and 2D linear modeling for a vertically incident plane wave. Note that 1D modeling captures most aspects of amplification in this profile, with a maximum amplification around 4 for all resonance frequencies. On the other hand, 2D results show larger amplification factors, around 6 for the fundamental frequency, and the basin effect between 1200 and 1400 m along the profile (between 8 and 10 Hz). However, 2D modeling shows the higher modes of the transfer function produced by the dipping layers of the basin at the left hand side of the model.

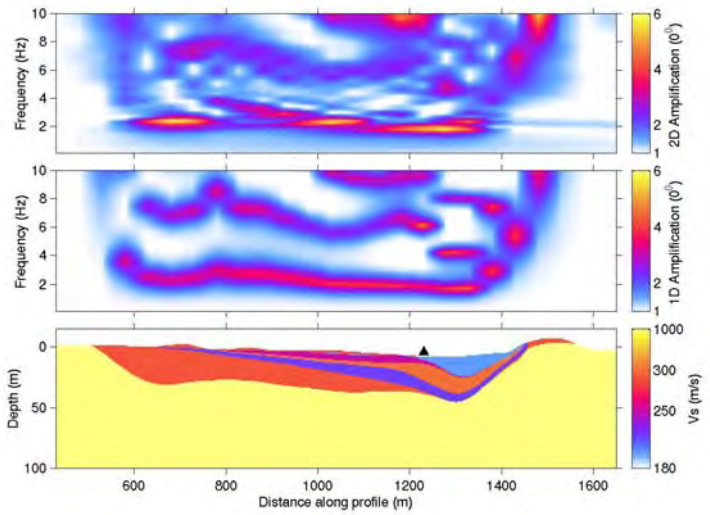

Figure 4: 2D (top) and 1D (middle) amplification transfer function for vertically incident plane wave. The black triangle shows the location of station NLIB.

Inclined incidence

Two plane waves coming from left to right (+35°) and from right to left (-35°) are introduced in the computations in order to see the effect of local seismicity. Figure 5 shows the corresponding amplification transfer functions. For comparison the transfer function for vertical incidence is also shown. For inclined incidence, the effect of the basin geometry is rather important, and the amplification factors are much higher than for vertical incidence. In addition, this amplification is broadband, something that cannot be seen in simple 1D models or even in 2D vertically incident computations. Finally, for -35°, there are topographical effects produced next to the small elevation around 1500 m along the profile. This feature acts a point injecting energy into the basin.

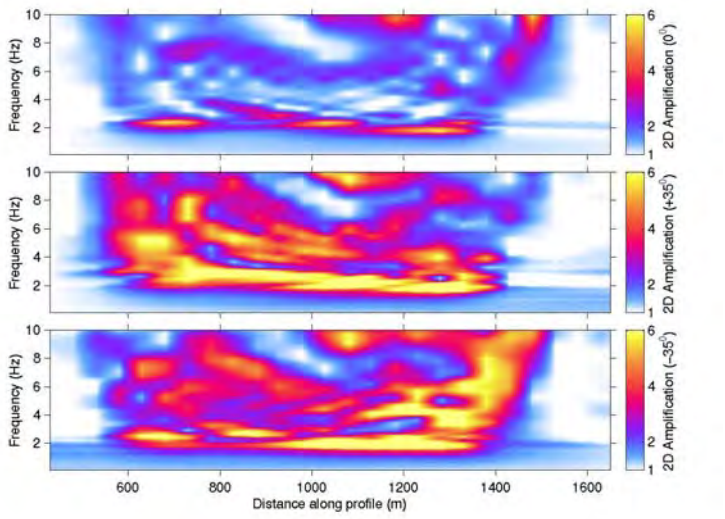

Figure 5: 2D amplification transfer function. (Top) vertical incidence. (Middle) 35° left to right inclined incidence. (Bottom) 35° right to left inclined incidence.

Aggravation factor

The aggravation factor is the ratio between 2D and 1D amplification transfer functions ([14]). Figure 6 shows the aggravation factor for two cases. The first (top) is for 2D vertical incidence wave propagation and the second (middle) for the geometric mean of vertical and inclined incidence. When having vertical incidence, both 1D and 2D models agree closely except in locations within the basin and at the basin edges. However, for inclined incidence, the aggravation factor is strongly affected by a factor of 4 to 6. These results show that the 1D amplification values are underestimated along the whole basin profile.

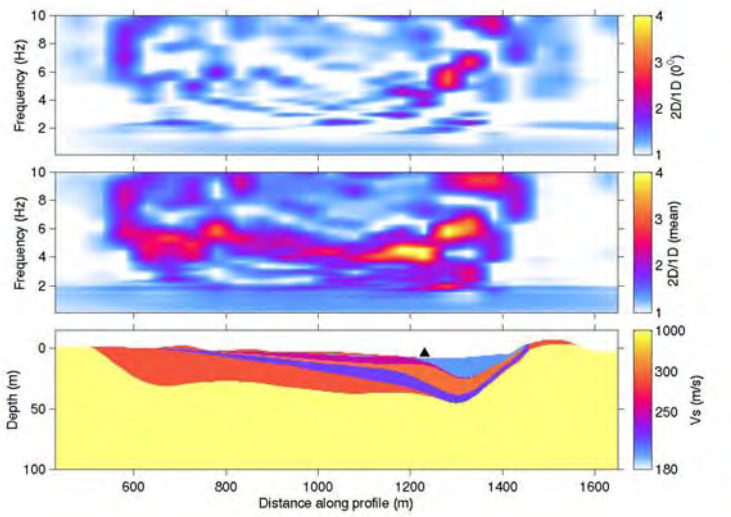

Figure 6: Aggravation factor for the Nice profile. (Top) 2D/1D aggravation factor for vertically incident wavefield. (Middle) ratio between the geometric mean of 2D amplification values for all angles of incidence and the 1D vertically incident wavefield.

2D P-SV nonlinear modeling

All previous computations were performed assuming wave propagation in viscoelastic linear media. However, it is widely known that soft soils behave nonlinearly. Indeed, this may be produced in the case of Nice since there is a strong impedance contrast between the sediments (around 300 m/s) and the bedrock (1000 m/s). Therefore wave propagation that takes into account nonlinear soil behavior is desirable. As it was stated above, the input ground motion is a synthetic acceleration time histories having a PGA of 0.2 g. With this kind of PGA it is likely to have nonlinear effects due to the low strength of the sediments and the strong impedance contrast. Figure 7 shows the amplification transfer function for the three angles of incidence of the incoming wavefield. The effect of soil nonlinearity is stronger in the case of vertically incident plane wave. Thus, we observe deamplification above 2Hz and shift of the resonant frequency to lower frequencies. These results show the importance of the angle of incidence and thickness of sediments for controlling the amount of nonlinear effects. Evidently, this cannot be modeled by 1D wave propagation only.

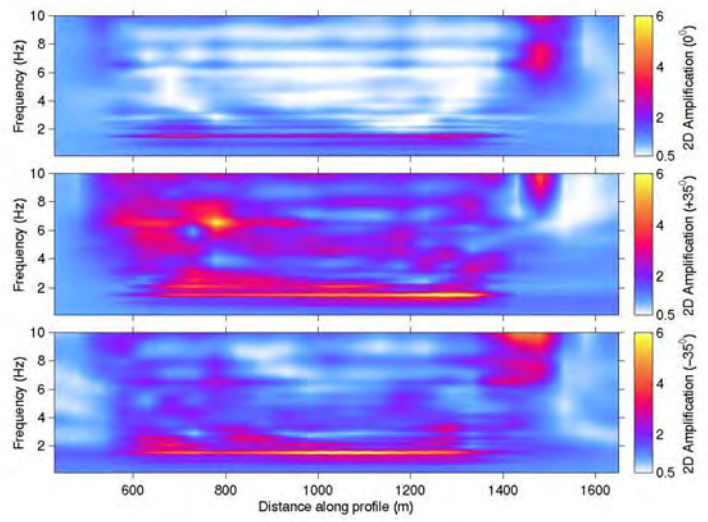

Figure 7: 2D amplification transfer function when nonlinear soil behavior is taken into account. (Top) vertical incidence. (Middle) 35° left to right inclined incidence. (Bottom) 35° right to left inclined incidence.

Conclusions

Saenger's stencil has proven to be a useful tool to model complex wave phenomena occurring in 2D basins including nonlinear soil behavior. The 2D basin of Nice has a strong impedance contrast between the sediments and the bedrock that strong amplification values may be present. This amplification is especially strong for inclined incoming wavefield. The effect of the angle of incidence is outstanding even in the case of nonlinear soil response. These results suggest that for complete evaluation of the seismic hazard, 2D and 3D modeling are needed to explore the full complexity of wave propagation and the corresponding basin response, which cannot be predicted by 1D studies.

References

[1] Olsen, K.B., and R.J. Archuleta (1996). 3D Simulation of Earthquakes on the Los Angeles Fault System, *Bull. Seism. Soc. Am.*, 86, 575 – 596.

[2] Satoh, T., H. Kawase, T. Sato, and A. Pitarka (2001). Three-Dimensional Finite-Difference Waveform Modeling of Strong Motions Observed in the Sendai Basin, Japan, *Bull. Seism. Soc. Am.*, 91, 812 – 825.

[3] Benites, R., and K.B. Olsen (2005). Modeling Strong Ground Motion in the Wellington Metropolitan Area, New Zealand, *Bull. Seism. Soc. Am.*, 97, 2180 – 2196.

[4] Saenger E., Gold N. and Shapiro S. (2000). Modeling the propagation of elastic waves using a modified finite-difference grid. *Wave Motion*, 31, 77-82.

[5] Gélis C., Leparoux D., Virieux J., Bitri A., Operto S. and Grandjean G., 2005. Numerical modelling of surface waves over shallow cavities. Journal of Environmental and Engineering Geophysics, 10, 49-59.

[6] Virieux J., 1986. P-SV wave propagation in heterogeneous media: velocity-stress finite-difference method. Geophysics, 51, 4, 889-901

[7] Day S. M. and Bradley C. R., 2001. Memory-efficient simulation of anelastic wave propagation. BSSA, 91, 3, 520-531.

[8] Towhata, I., and K. Ishihara (1985). Modeling Soil Behavior Under Principal Axes Rotation, Fifth International Conference on Numerical Methods in Geomechanics, Nagoya, 523-530.

[9] Iai, S., Y. Matsunaga, and T. Kameoka (1990a). Strain Space Plasticity Model for Cyclic Mobility, Report of the Port and Harbour Research Institute, 29, 27-56.

[10] Iai, S., Y. Matsunaga, and T. Kameoka (1990b). Parameter Identification for Cyclic Mobility Model, Report of the Port and Harbour Research Institute, 29, 57-83.

[11] Konder, R.L., and J.S. Zelasko (1963). A hyperbolic stress-strain formulation for sands, in Proc. of 2nd Pan American Conference on Soil Mechanics and Foundation Engineering, Brazil, 289-324.

[12] Duval, A.M. (1996). Détermination de la réponse d'un site aux séismes à l'aide du bruit de fond - Evaluation expérimentale, *Rapport Etudes et Recherches des Laboratoires des Ponts et Chaussées*, n°GT62, 264 p., LCPC, Paris.

[13] GEMGEP phase 1 (2000). Risque sismique sur Nice: étude de scénarios de gestion de crise sismique. Définition de l'aléa, de la vulnérabilité et des enjeux. *CETE Méditerranée, laboratoire de Nice*.

[14] Makra K., F.J. Chavez-Garcia, Raptakis D., Pilitakis K. (2001). Parametric analysis of the seismic response of a 2D sedimentary valley: implications for code implementations of complex site effects, Soil dynamics and earthquake engineering, 25, 303-315.